Inorg. Chem. **2009**, *48*, 1655−1660

Photofragmentation Pathways and Photodeposition of Nanoparticles from a Gas Phase Copper-Containing Precursor

Philip X. Rutkowski and Jeffrey I. Zink*

Department of Chemistry and Biochemistry, University of California, Los Angeles, Los Angeles, California 90095

Received November 8, 2008

Pulsed laser excitation of bis(2,2,6,6-tetramethyl-3,5-heptanedionato)copper(II) ($Cu(TMHD)_2$) in the gas phase produced neutral gaseous copper atoms and nanoparticulate copper deposits on substrates. Copper atoms were formed by the complete dissociation of the ligands from the metal. Time of flight mass spectrometry and resonance enhanced multiphoton ionization spectroscopy were used to study the details of this reaction and led to the discovery of other gaseous fragments that were produced by incomplete fragmentation of the ligands including monoligated species and coordinated ligand fragments. Laser-assisted chemical vapor deposition resulted in monodispersed nanoparticles under 100 nm in diameter. X-ray photoelectron spectroscopy and energy dispersive analysis of X-rays were used to determine the elemental composition of the deposit. The relationships between the photofragmentation pathways and the deposited particles are discussed.

Introduction

Photodeposition of copper from gas phase precursors has been extensively studied. Copper has been photodeposited in the form of nanoparticles and thin films using UV and visible light excitation from a small number of precursors.[1] The bulk of the research on copper precursors was done on Cu(hfac)(TMVS) (hfac = 1,1,1,5,5,5-hexafluoro-2,4-pentanedionato; TMVS = trimethylsilylethene),[2−6] $Cu(hfac)_2$,[7−12] and $Cu(TMHD)_2$.[11−16] Other copper precursors that have been studied include Cu(hfac)(COD) (COD = 1,5-cyclooctadiene),[17] Cu(hfac)(MHY) (MHY = 2-methyl-1-hexene-3-yne),[18] $Cu(acac)_2$ (acac = 2,4-pentanedionato),[19] $CuCp(Et_3P)$ (Cp = cyclopentadienyl; Et_3P = triethylphosphine),[20] $Cu(tfa)_2$ (tfa = 1,1,1-trifluoro-5,5-dimethyl-2,4-hexanedionato),[21] and $Cu(baa)_2$ (baa = *tert*-butylacetoacetato).[22]

Recent studies in gas phase photochemistry of metal-containing chemical vapor deposition (CVD) precursors monitored by mass spectrometry have uncovered unique

* To whom correspondence should be addressed. E-mail: zink@chem.ucla.edu. Tel: 310-825-1001. Fax: 310-206-4038.

(1) Maury, F.; Vidal, S.; Gleizes, A. *Adv. Mater. Opt. Electron.* **2000**, *10*, 123–133.
(2) Han, J.; Jensen, K. F.; Norman, J. A. T. *Mater. Res. Soc. Symp. Proc.* **1992**, *236*, 97–104.
(3) Izquierdo, R.; Bertomeu, J.; Suys, M.; Sacher, E.; Meunier, M. *Appl. Surf. Sci.* **1995**, *86*, 509–513.
(4) Widmer, M.; van den Bergh, H. *J. Appl. Phys.* **1995**, *77*, 5464–5466.
(5) Moilanen, H.; Remes, J.; Leppävuori, S. *Phys. Scr.* **1997**, *T69*, 237–241.
(6) Wu, Y.-L.; Hsieh, M.-H.; Hwang, H.-L. *Thin Solid Films* **2005**, *483*, 10–15.
(7) Jones, C. R.; Houle, F. A.; Kovac, C. A.; Baum, T. H. *Appl. Phys. Lett.* **1985**, *46*, 97–99.
(8) Markwalder, B.; Widmer, M.; Braichotte, D.; van den Bergh, H. *J. Appl. Phys.* **1989**, *65*, 2470–2474.
(9) Preuss, S.; Stafast, H. *Appl. Phys. A: Mater. Sci. Process.* **1992**, *54*, 152–157.
(10) Chen, Y. D.; Reisman, A.; Turlik, I.; Temple, D. *J. Electrochem. Soc.* **1995**, *142*, 3911–3918.
(11) Karsi, M.; Reynes, A.; Morancho, R. *J. Phys. IV* **1993**, *3* (C3), 273–280.
(12) Suys, M.; Moffat, B.; Bernier, M.-H.; Izquierdo, R.; Poulin, S.; Meunier, M.; Sacher, E. *Mater. Res. Soc. Symp. Proc.* **1993**, *282*, 179–184.
(13) Hashimoto, T.; Kitazawa, K.; Nakabayashi, M.; Shiraishi, T.; Suemune, Y.; Yamamoto, T.; Koinuma, H. *Appl. Organomet. Chem.* **1991**, *5*, 325–330.
(14) Ushida, T.; Higashiyama, K.; Hirabayashi, I.; Tanaka, S. *Jpn. J. Appl. Phys.* **1991**, *30*, L35−L38.
(15) Koinuma, H.; Chaudhary, K.; Nakabayashi, M.; Shiraishi, T.; Hashimoto, T.; Kitazawa, K.; Suemune, Y.; Yamamoto, T. *Jpn. J. Appl. Phys.* **1991**, *30*, 656–660.
(16) Zama, H.; Miyake, T.; Hattori, T.; Oda, S. *Jpn. J. Appl. Phys.* **1992**, *31*, L588−L590.
(17) Vidal, S.; Maury, F.; Gleizes, A.; Mijoule, C. *Appl. Surf. Sci.* **2000**, *168*, 57–60.
(18) Vidal, S.; Maury, F.; Gleizes, A.; Chen, T.-Y.; Doppelt, P. *J. Phys. IV* **1999**, *9* (Pr8), 791–798.
(19) Tonneau, D.; Pierrisnard, R.; Dallaporta, H.; Marine, W. *J. Phys. IV* **1995**, *5* (C5), 629–635.
(20) Dupuy, C. G.; Beach, D. B.; Hurst, J. E., Jr.; Jasinski, J. M. *Chem. Mater.* **1989**, *1*, 16–18.
(21) Mao, D.-M.; Jin, Z.-K.; Qin, Q.-Z. *J. Appl. Phys.* **1992**, *71*, 6111–6115.
(22) Cheon, J.; Zink, J. I. *Inorg. Chem.* **2000**, *39*, 433–436.

10.1021/ic802138p CCC: $40.75 © 2009 American Chemical Society
Published on Web 01/21/2009

photofragmentation patterns.[23−32] Although the atomic metal species tend to be the dominant products, other metal-containing photofragments can form as well. The formation of these fragments can be enhanced under certain conditions such as optimal wavelengths and laser power.[23,24,27−31] A correlation between the photodeposits and these photofragmentation patterns would prove to be useful.

Although many studies have analyzed the photodeposited copper films, research about the photochemical mechanisms leading to the formation of the deposits is scarce. A time of flight mass spectrometry (TOF-MS) study on $Cu(hfac)_2$ using photoionization suggested that ligand fragments could contribute to the photodeposits in copper films deposited by laser-assisted chemical vapor deposition (LCVD).[33] However, no investigations into the detailed photofragmentation pathways of gas phase copper-containing LCVD precursors have been reported. This research would provide insight into which ligand atoms could be incorporated in metal films, which mechanisms the precursor could follow to produce the deposits, and better precursor and wavelength selection to avoid unwanted byproduct.

In this work, we report on the photofragmentation pathways and the photodeposition of bis(2,2,6,6-tetramethyl-3,5-heptanedionato)copper(II) ($Cu(TMHD)_2$). The gas phase photofragments were deposited onto a silicon substrate using both UV and visible excitation and were examined by scanning electron microscopy (SEM), energy dispersive analysis of X-rays (EDAX), and X-ray photoelectron spectroscopy (XPS). The results showed a strong atomic copper presence with smaller amounts of copper oxide and copper carbide. TOF-MS was used to characterize the photofragmentation of the compound. The dominant metal-containing ion detected using UV and visible excitation was Cu^+. Other metal-containing fragments, including CuC^+ and CuO^+, were also discovered, leading us to elucidate detailed photofragmentation pathways that suggest how the photodeposits were created.

Experimental Section

Materials. Bis(2,2,6,6-tetramethyl-3,5-heptanedionato)copper(II) was purchased from Strem and used without any further purification.

Spectroscopy. Photoionization mass spectra were measured in a TOF mass spectrometer that was constructed based on a design in the literature.[34] UV excitation was performed at 355 nm (∼60 mJ/pulse, $\sim 10^9$ W/cm^2) using a Quantel Brilliant Nd:YAG laser. Visible excitation was achieved using an OPOTEK optical parametric oscillator pumped by the third harmonic of the Nd:YAG laser in the range of 410−680 nm (∼30 mJ/pulse, $\sim 10^8$ W/cm^2, 6 ns pulse width, 10−20 cm^{-1} bandwidth). An optical KV-389 filter is used to eliminate residual pump (355 nm) from the visible laser beam. Photoionization occurs in a stainless steel cube (30 cm edges) equipped with quartz windows and evacuated to less than 10^{-6} Torr by a 6 in. diffusion pump fitted with a water cooled baffle. The precursor is sublimed to 80 °C and enters the chamber entrained in He with a backing pressure of 10^3 Torr through a pulsed nozzle. The high speed solenoid valve (General Valve series 9, 0.5 mm orifice) sends a 0.2 ms pulse of the sample to intersect the ionization laser beam at 90° between two accelerator plates. The fragment ions are accelerated through a 1 m flight tube kept at 10^{-5} Torr using a Varian V300HT 6 in. air cooled turbomacromolecular pump. The voltages on the accelerator plates are 3000 V, 2100 V, and ground, respectively, in order from farthest to nearest the detector. Ions are detected using a 40 mm diameter triple microchannel plate detector assembly (Jordan TOF Products, Inc.) set at −3400 V. The ion signal is processed using a Tektronix TDS2022 200 MHz dual channel digital oscilloscope interfaced with a PC.

Gas phase luminescence spectra were obtained in an evacuated stainless steel six-way cross with synthetic fused silica windows. A sample of the precursor is placed in a glass U-tube with Teflon needle valves. The U-tube and six-way cross are heated to approximately 80 °C and the sublimed precursor is seeded with a carrier gas (He) before the gaseous mixture enters the chamber. The six-way cross is also fitted with a roughing pump that maintains a medium vacuum inside the chamber. The focused output of the Nd:YAG laser excites the gaseous sample, and the emitted light is collected at right angles and directed into a 0.32 m monochromator (Instruments SA, Inc., HR320). The emitted photons are dispersed by a 600 groove/mm holographic grating and detected by a Princeton Instruments ICCD camera (PI-Max 1024RB).

Deposition and Characterization. Photodeposition was performed on a silicon wafer (Sb doped, 100 orientation, 0.005−0.02 Ω resistivity, 475−575 μm thick) using the same setup as that in the gas phase luminescence experiments. SEM images were collected on a JEOL JSM-6700F field emitting scanning electron microscope equipped with an EDAX detector. The nanoparticles created from the photodeposition were coated with gold using a sputterer (Hummer 6.2, Anatech LTD, plasma discharge current = 15 mA at 70 mTorr) before they were examined by SEM. XPS spectra of the samples were collected with a PHI 3057 spectrometer using aluminum Kα X-rays at a 25° detection angle with respect to the surface normal.

Results and Discussion

I. Photodeposition. LCVD of $Cu(TMHD)_2$ was used to deposit nanoparticulate Cu with UV and visible excitation. Using pulsed UV excitation (355 nm, ∼60 mJ/pulse), deposits began forming almost immediately on the silicon substrate. A slightly unfocused beam was used to prevent ablation of the silicon. However, because of much lower power output (∼30 mJ/pulse) from the laser using the OPO and weaker molecular absorption in the visible, a focused beam was used to deposit the precursor with visible excitation

(23) Muraoka, P.; Byun, D.; Zink, J. I. *J. Am. Chem. Soc.* **2000**, *122*, 1227–1228.
(24) Muraoka, P.; Byun, D.; Zink, J. I. *Coord. Chem. Rev.* **2000**, *208*, 193–211.
(25) Jaeger, T. D.; Duncan, M. A. *J. Phys. Chem. A* **2004**, *108*, 11296–11301.
(26) Jaeger, T. D.; Duncan, M. A. *Int. J. Mass Spectrom.* **2005**, *241*, 165–171.
(27) Ow, F. P.; Berry, M. T.; May, P. S.; Zink, J. I. *J. Phys. Chem. A* **2006**, *110*, 7751–7754.
(28) Ow, F. P.; Berry, M. T.; May, P. S.; Zink, J. I. *J. Phys. Chem. A* **2007**, *111*, 4144–4149.
(29) Ow, F. P.; Henderson, B.; Zink, J. I. *Inorg. Chem.* **2007**, *46*, 2243–2248.
(30) Muraoka, P.; Byun, D.; Zink, J. I. *J. Phys. Chem. A* **2001**, *105*, 8665–8671.
(31) Byun, D.; Zink, J. I. *Inorg. Chem.* **2003**, *42*, 4308–4315.
(32) Talaga, D. S.; Zink, J. I. *Inorg. Chem.* **1996**, *35*, 5050–5054.
(33) Bartz, J. A.; Galloway, D. B.; Huey, L. G.; Glenewinkel-Meyer, T.; Crim, F. F. *J. Phys. Chem.* **1993**, *97*, 11249–11252.
(34) Wiley, W. C.; McLaren, I. H. *Rev. Sci. Instrum.* **1955**, *26*, 1150–1157.

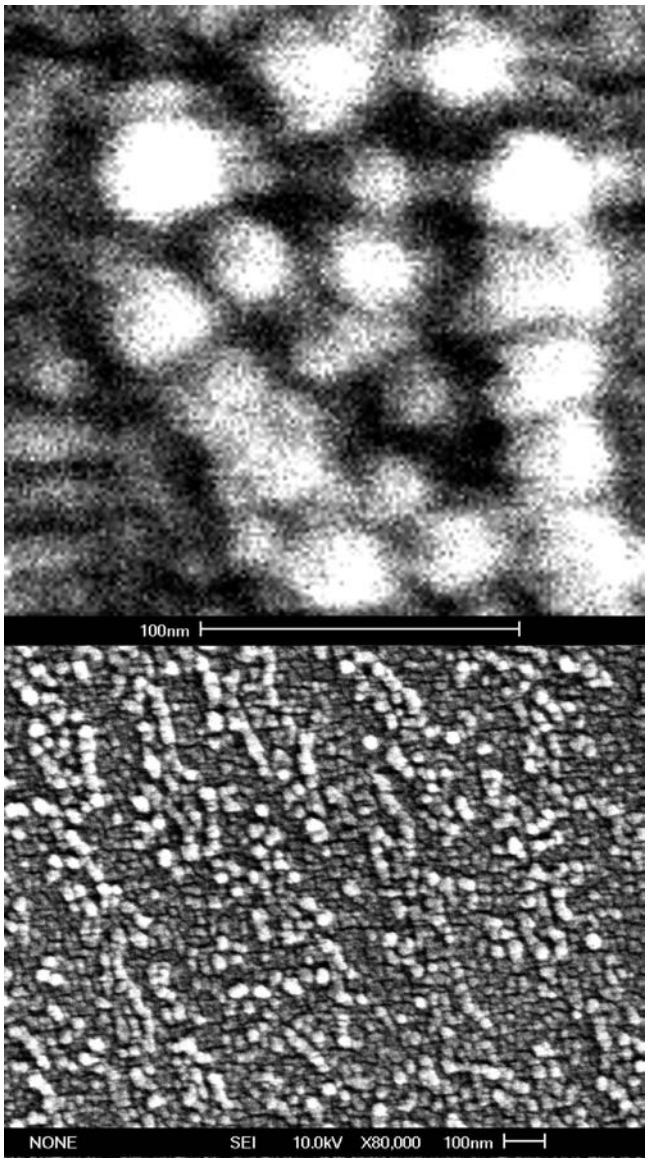

Figure 1. SEM images of photodeposited copper nanoparticles on a silicon substrate using visible excitation.

(413 nm). Deposition time using visible excitation was an order of magnitude longer (~3 min) than that for UV excitation.

The deposits created from UV and visible excitation formed nanoparticles on the surface of the silicon substrate. SEM scans showed that the sizes of the nanoparticles were under 100 nm in diameter as seen in Figure 1. The only observable difference of the surface morphologies between the deposits resulting from UV and visible excitation was that the UV excitation created more nanoparticles and eventually began to form a smoother metallic surface.

Analysis of the composition of both the UV and the visible photodeposits yielded similar results. XPS and EDAX spectra showed a strong copper signal in both types of deposits. In addition, the presence of oxygen and carbon on the surface was observed. As seen in Figure 2, the data obtained from XPS show clear CuO signals in addition to atomic Cu. The CuO signals could indicate that a small oxide monolayer formed above the deposited copper when the substrate was exposed to air. The XPS results also show a small shoulder near the CuO peak which could indicate the presence of CuC. The CuC presence may result from incomplete photofragmentation in the gas phase and depositing carbon-containing fragments onto the silicon substrate.

The particles formed by LCVD are surprisingly uniform in size. Kinetic studies of Au and Cu nanoparticles and ZnCdSe quantum dots deposited by thermal CVD have attributed their formation to Ostwald ripening.[35−37] The Ostwald ripening process explains how small nanoparticles evolve to form larger nanoparticles. Molecules on the surface of a particle are less energetically favorable than molecules inside the framework of the particle and, as a result, attract other molecules to form a larger framework.

II. Photofragmentation Studies. TOF-MS studies of $Cu(TMHD)_2$ in the gas phase revealed a very strong presence of Cu^+. Using visible excitation, Cu^+ had the greatest signal intensity surpassing that of *t*-butyl$^+$. Other ions that were produced included heavier copper-containing fragments that yielded a much lower signal intensity and will be discussed later in Section III. Using UV excitation, the Cu^+ signal was not the most prominent. Instead, the *t*-butyl fragment had the highest signal intensity. *t*-Butyl photodissociation is a known mechanism among TMHD precursors.[38] Similar to the results obtained using visible excitation, heavier copper-containing ion fragments were also detected but with less signal intensity. The heavy mass ions were more prominent using visible excitation than using UV excitation because of lower photon energies and pulse energies from the laser. Figure 3 shows a typical TOF-MS spectrum from blue (413 nm) excitation.

Wavelength dependent photofragmentation studies were also performed on this molecule. The resonance enhanced multiphoton ionization (REMPI) spectrum of the Cu^+ signal intensity as a function of wavelength is shown in Figure 4. Sharp peaks corresponding to neutral copper atom transitions were observed. Neutral atomic copper can be ionized if the monatomic species is excited with three photons or more of wavelengths less than 480 nm. The Cu^0 transitions that were observed occurred at known atomic copper absorptions of 428 nm ($4p'\ ^4P^0 - 5s'\ ^4D$), 453 nm ($4p\ 2P^0 - 6s\ ^2S$), and 465 nm ($4p'\ ^4F^0 - 5s'\ ^4D$).[39,40] The presence of these Cu^0 lines in the REMPI spectrum are proof that neutral copper atoms are formed in the gas phase.

Luminescence studies of the precursor in the gas phase also showed known emission lines from excited states of

(35) LaLonde, A. D.; Norton, M. G.; Zhang, D.; Gangadean, D.; Alkhateeb, A.; Padmanabhan, R.; McIlroy, D. N. *J. Mater. Res.* **2005**, *20*, 3021–3027.
(36) Zhang, H.; Goodner, D. M.; Bedzyk, M. J.; Marks, T. J.; Chang, R. P. H. *Chem. Phys. Lett.* **2004**, *395*, 296–301.
(37) Shan, C. X.; Fan, X. W.; Zhang, J. Y.; Zhang, Z. Z.; Li, B. S.; Lu, Y. M.; Liu, Y. C.; Shen, D. Z.; Kong, X. G.; Wang, X. H. *J. Vac. Sci. Technol. B* **2002**, *20*, 1102–1106.
(38) Fukuda, E. K.; Campana, J. E. *Int. J. Mass Spectrom. Ion Processes* **1985**, *65*, 321–328.
(39) Meggers, W. F.; Corliss, C. H.; Scribner, B. F. *Tables of Spectral-Line Intensities Part I - Arranged by Elements*, 2nd ed.; U.S. Government Printing Office: Washington, DC, 1975.
(40) Striganov, A. R.; Sventitskii, N. S. *Tables of Spectral Lines of Neutral and Ionized Atoms*; IFI/Plenum: New York, 1968.

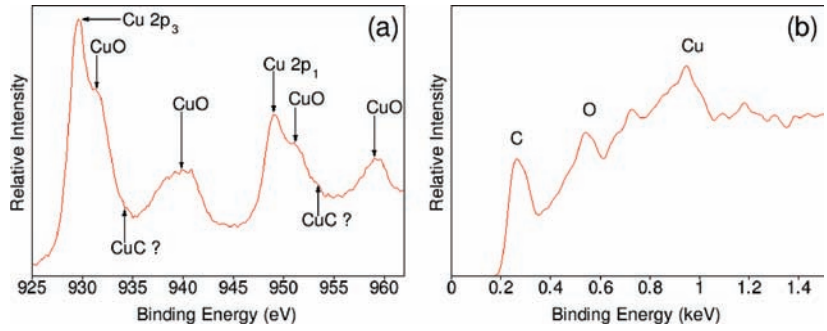

Figure 2. XPS (a) and EDAX (b) characterization of the photodeposits using visible excitation.

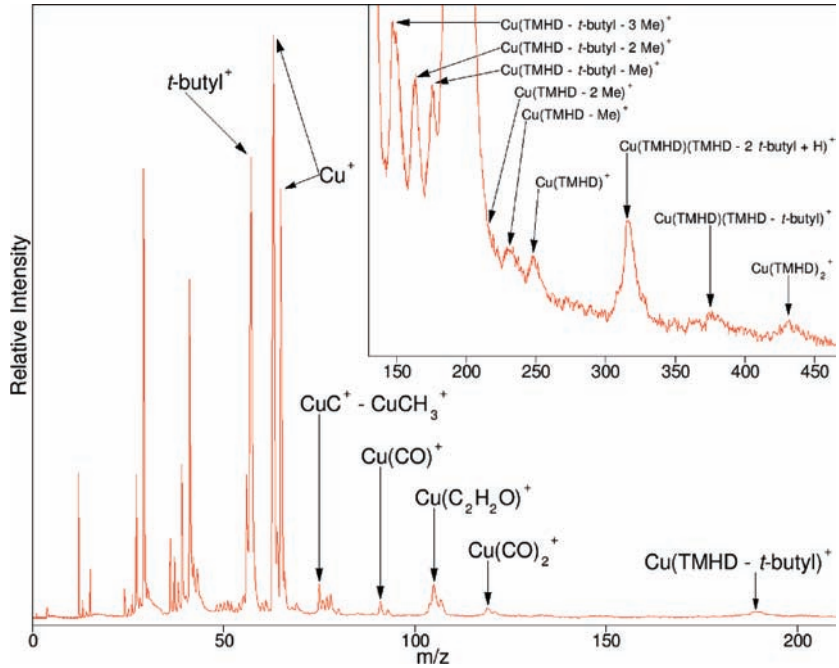

Figure 3. TOF-MS spectra from the 413 nm excitation of $Cu(TMHD)_2$. The weaker large mass peaks are shown in the inset.

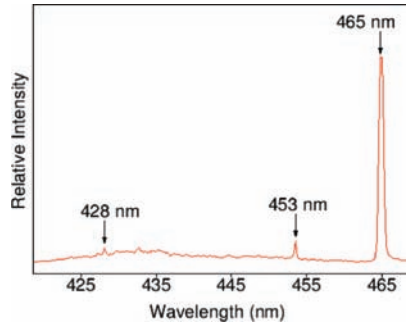

Figure 4. REMPI spectrum of Cu^+ formation vs excitation wavelength. The arrows show resonances with neutral atomic copper transitions (428 nm = $4p'\ ^4P^0 - 5s'\ ^4D$, 453 nm = $4p\ 2P^0 - 6s\ ^2S$, and 465 nm = $4p'\ ^4F^0 - 5s'\ ^4D$).

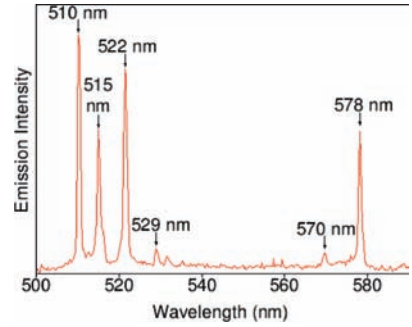

Figure 5. Gas phase luminescence spectrum observed from the excitation of $Cu(TMHD)_2$ at 355 nm. The arrows indicate neutral atomic copper transitions (510 nm = $4s^2\ ^2D - 4p\ ^2P^0$, 5/2 − 3/2 J, 515 nm = $4p\ ^2P^0 - 4d\ ^2D$, 1/2 − 3/2 J, 522 nm = $4p\ ^2P^0 - 4d\ ^2D$, 3/2 − 5/2 J, 529 nm = $4p'\ ^4D^0 - 5s'\ ^4D$, 7/2 − 7/2 J, 570 nm = $4s^2\ ^2D - 4p\ ^2P^0$, 3/2 − 3/2 J, and 578 nm = $4s^2\ ^2D - 4p\ ^2P^0$, 3/2 − 1/2 J).

neutral atomic copper. As seen in Figure 5, the known transitions that were observed occurred at 510 nm ($4s^2\ ^2D - 4p\ ^2P^0$, 5/2 − 3/2 J), 515 nm ($4p\ ^2P^0 - 4d\ ^2D$, 1/2 − 3/2 J), 522 nm ($4p\ ^2P^0 - 4d\ ^2D$, 3/2 − 5/2 J), 529 nm ($4p'\ ^4D^0 - 5s'\ ^4D$, 7/2 − 7/2 J), 570 nm ($4s^2\ ^2D - 4p\ ^2P^0$, 3/2 − 3/2 J), and 578 nm ($4s^2\ ^2D - 4p\ ^2P^0$, 3/2 − 1/2 J).[39,40] These results provide further evidence of the formation of neutral copper in the gas phase by the complete dissociation of the TMHD ligands.

III. Pathways to Cu. TOF-MS studies also revealed sequential fragmentation patterns where the precursor molecule sheds pieces of the ligand producing large metal-containing ions. From these ions, detailed photofragmentation pathways were determined.

The heaviest masses and most prominent peaks were formed from the loss of *t*-butyl groups from each ligand (Figure 6a). As shown previously in studies of this compound

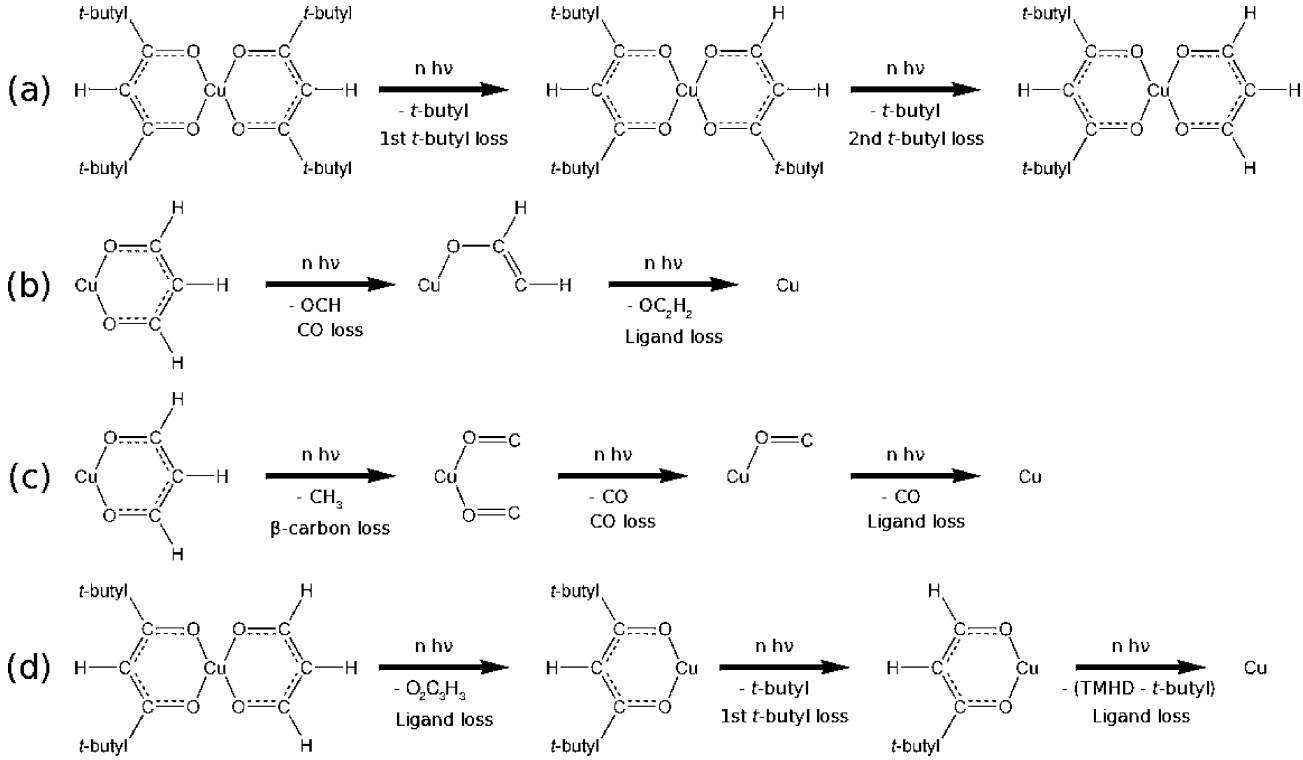

Figure 6. Photofragmentation pathways: (a) sequential *t*-butyl loss; (b) CO loss from the ligand fragment produced in (a); (c) β-carbon loss from the ligand fragment produced in (a); and (d) complete ligand loss.

using either photons or electrons as the ionization source, the loss of a *t*-butyl group from a TMHD ligand is an important step to reaching the formation of neutral copper.[41−44] As a *t*-butyl group dissociates, a hydrogen atom from the dissociated *t*-butyl takes its place. This mechanism has been reported using electroionization mass spectrometry.[44] The replacement of a *t*-butyl with a hydrogen atom would not have been observed without the dissociation of the second *t*-butyl. Without this replacement, $Cu(C_3HO_2)^+$ (132 *m*/*z*) would be an expected fragment, but $Cu(C_3H_2O_2)^+$ (133 *m*/*z*) is the observed ion fragment. All four fragments following this type of dissociation were observed and varied in intensity with Cu(TMHD − *t*-butyl)$^+$ being the largest followed by Cu(TMHD − 2 *t*-butyl + H)$^+$, Cu(TMHD)(TMHD − 2 *t*-butyl + H)$^+$, and Cu(TMHD)(TMHD − *t*-butyl)$^+$. In Figure 6a, the photofragment, Cu(TMHD)(TMHD − 2 *t*-butyl + H)$^+$, is shown as having lost two *t*-butyl groups from one ligand. It is not known whether the second *t*-butyl group fragment is from the same ligand as the first one or from the other intact ligand, because the results obtained from TOF-MS return mass units and not structure.

Another very important dissociation step is the loss of a CO group (Figure 6b). This fragmentation step only occurs after the second *t*-butyl loss; Cu(OCHCHCO)$^+$ becomes Cu(OCHCH)$^+$. This step must occur after the loss of the second *t*-butyl from the fragmenting ligand because the fragment Cu(OC*t*BuCH)$^+$ was not observed. This dissociation step was observed with a varying number of bonded hydrogens ranging from zero to three hydrogens.

In addition to CO loss, another dissociation step that can occur after the loss of both *t*-butyl groups from one ligand is the loss of the β carbon (Figure 6c). The Cu(OCHCHCO)$^+$ ion fragment can lose CH_2, which results in the formation of $Cu(OC)_2^+$. Further fragmentation can lead to the formation of Cu(OC)$^+$ and CuO$^+$, which was also observed. Again, the ion fragment $Cu(OCtBu)_{1,2}^+$ was not observed indicating that this step must occur after the loss of the second *t*-butyl.

Some ions appeared only in trace amounts and under extremely sensitive detection conditions, indicating that the pathway leading to their formation occurs infrequently. The loss of a methyl group from a coordinated TMHD ligand is one example. The fragments (Cu(TMHD) − 1, 2, and 3 Me)$^+$ and (Cu(TMHD) − *t*-butyl − 1, 2, and 3 Me)$^+$ were the only ions detected originating from this kind of dissociation. These ion fragments were detected in trace amounts when the negative voltage on the detector plates was increased, and because of their extremely low intensities, they are not significant to the overall fragmentation of the molecule.

Inevitably, a final route to the formation of Cu is complete ligand loss (Figure 6b−d). This can happen at any point along the photofragmentation pathway. The coordinated fragmenting ligands previously mentioned were observed as fragments themselves including (TMHD − *t*-butyl)$^+$, (TMHD − 2 *t*-butyl + H)$^+$, $(C_2H_2O)^+$, and (OC)$^+$.

IV. Pathways to CuO and CuC. The photofragmentation pathways determined from TOF-MS scans exposed possible pathways for the formation of the oxygen and carbon

(41) Bykov, A. F.; Semyannikov, P. P.; Igumenov, I. K. *J. Therm. Anal.* **1992**, *38*, 1463–1475.
(42) Mukhopadhyay, S.; Shalini, K.; Devi, A.; Shivashankar, S. A. *Bull. Mater. Sci.* **2002**, *25*, 391–398.
(43) Schildcrout, S. M. *Inorg. Chem.* **1980**, *19*, 224–227.
(44) Jiang, Y.; Liu, M.; Wang, Y.; Song, H.; Gao, J.; Meng, G. *J. Phys. Chem. A* **2006**, *110*, 13479–13486.

presence detected in the XPS and EDAX studies. XPS showed that CuO was the origin of the oxygen that was detected in EDAX. Carbon was also discovered in the thin films and, according to the XPS data, was possibly bonded directly to copper.

The detection of CuO could be the result of a thin oxide film that formed when the substrate was exposed to air. But since the CuO^+ fragment was detected in the TOF-MS scans, it is also possible that the CuO in the deposits could have been partly due to the formation of CuO by photofragmentation. There are two possible pathways that could lead to this end product. After both *t*-butyl groups are lost, the loss of the β carbon leaves a copper-containing fragment with two coordinated CO groups. Further fragmentation can possibly lead to the CuO contamination that was observed. Another possibility is that a CO group is lost after both *t*-butyl groups are lost, and another copper-containing fragment is formed with a coordinated C_2H_xO group. Again, further fragmentation can lead to the CuO presence.

In the XPS scans, a very small presence of CuC was also observed. CuC^+ is observed in the gas phase. Since no carbon is directly bonded to the copper atom in the precursor molecule, the CuC presence could be a result of an internal rearrangement observed in previous studies of other β-diketonate precursors.[45] The mechanism that was discussed involved metal oxygen bond cleavage followed by an interaction between the β carbon and the metal. Further excitation of this fragment could lead to CuC extraction.

V. Unusual Photofragments. In addition to the photofragments that form from sequential ligand degradation, unusual small ion fragments were observed in the TOF-MS studies. Metal diatomics form one important group. CuH^+ (as well as triatomic CuH_2^+) were seen using UV and visible excitation and are believed to be formed by the same internal rearrangement mechanism that leads to CuC. CuC^+ (as well as $CuCH^+$, $CuCH_2^+$, and $CuCH_3^+$) was observed using UV and visible excitation, and its formation was discussed previously. Lastly, CuO^+ was seen with both UV and visible excitation and is believed to be a result of further fragmentation of the products of either the CO loss or the β-carbon loss. All three diatomic photofragments were observed with significant intensities equal to or greater than those of the heavier copper-containing ions.

Another set of unusual photofragments consists of the products of the CO loss and β-carbon loss mechanisms. After the second *t*-butyl group dissociates from one of the ligands, CO loss can occur and results in $Cu(OC_2H_{0-3})^+$. The structure of this photofragment and the placement of the hydrogens are not clear. Since a *t*-butyl group is replaced with a hydrogen, it is assumed that at least one of the hydrogens is bonded to the α carbon while the other one or two hydrogens are bonded to the β carbon in the three hydrogen fragment. However, all three hydrogens could be bonded to the β carbon. The structure of this photofragment cannot be determined from the TOF-MS. Another possible mechanism that could occur after losing a second *t*-butyl is β-carbon loss. The resulting photofragment is $Cu(CO)_2^+$. Again, the bonding cannot be determined by relying solely on the TOF-MS studies, but the $Cu(CO)_2^+$ cation was observed with clear Cu isotopic ratios.

Summary

The photofragments from the LCVD of $Cu(TMHD)_2$ were deposited onto a silicon substrate. SEM images showed the formation of sub-100 nm nanoparticles on the substrate. EDAX and XPS spectra revealed a strong presence of Cu in the nanoparticles along with CuO and CuC. The TOF-MS scans of $Cu(TMHD)_2$ revealed a strong presence of Cu^+ formed in the gas phase by the complete photodissociation of the ligands. The REMPI scans proved that neutral atomic copper is formed in the gas phase by the enhanced formation of Cu^+ when transitions of Cu^0 at wavelengths of 428 nm, 453 nm, and 465 nm were excited. Gas phase luminescence spectra of this precursor further confirmed the formation of atomic copper in the gas phase by the detection of known resonances of excited states of neutral atomic copper at wavelengths of 510 nm, 515 nm, 522 nm, 529 nm, 570 nm, and 578 nm. Detailed photofragmentation pathways that lead to Cu, CuO, and CuC were discussed on the basis of the copper-containing photofragments detected in TOF-MS scans.

Acknowledgment. This work was made possible by a grant from the National Science Foundation (CHE-0809384). The authors thank Professor Robert F. Hicks and Robyn Woo in the Department of Materials Science and Engineering for the use of their XPS instrument and helpful discussions.

IC802138P

(45) Muraoka, P.; Byun, D.; Zink, J. I. *Coord. Chem. Rev.* **2000**, *208*, 193–211.